

# Cross-sensor Pore Detection in High-resolution Fingerprint Images using Unsupervised Domain Adaptation

Vijay Anand, *Student Member, IEEE*, and Vivek Kanhangad, *Senior Member, IEEE*

**Abstract**—With the emergence of the high-resolution fingerprint sensors, research community has focused on level-3 fingerprint features especially, pores for providing the next generation automated fingerprint recognition system (AFRS). Following the recent success of the deep learning approaches in various computer vision tasks, researchers have explored learning-based approaches for pore detection in high-resolution fingerprint images. These learning-based approaches provide better performance than the hand-crafted feature-based approaches. However, domain adaptability of existing learning-based pore detection methods has not been examined in the past. In this paper, we present the first study of domain adaptability of existing learning-based pore detection methods. For this purpose, we have generated an in-house ground truth dataset referred to as IITI-HRF-GT by using 1000 dpi fingerprint sensor and evaluated the performance of the existing learning-based pore detection approaches on it. Further, we have also proposed an approach for detecting pores in a cross sensor scenario referred to as DeepDomainPore using unsupervised domain adaptation technique. Specifically, DeepDomainPore is combination of a convolutional neural network (CNN) based pore detection approach DeepResPore and an unsupervised domain adaptation approach included during the training process. The domain adaptation in the DeepDomainPore is achieved by embedding a gradient reversal layer between the DeepResPore and a domain classifier network. The results of all the existing and the proposed learning-based pore detection approaches are evaluated on IITI-HRF-GT. The DeepDomainPore provides a true detection rate of 88.09% and an F-score of 83.94% on IITI-HRF-GT. Most importantly, the proposed approach achieves state-of-the-art performance on the cross sensor dataset.

**Index Terms**—Pore detection, high-resolution fingerprint sensor, domain adaptation.

## I. INTRODUCTION

**P**ORES, which are level-3 fingerprint features, are generally observable in high-resolution fingerprint images of resolution higher than 800 dpi [1]. With the advancement in fingerprint sensing technology, researchers have focused their attention on level-3 fingerprint features especially, pores and proposed various next generation automated fingerprint recognition system (AFRS) [2]–[14]. Pore features have been found to carry sufficient discriminating power and they have also shown to be effective for recognition using partial fingerprint images, which may not contain sufficient level-2 features [7]. The performance of pore-based AFRS majorly depends on the pore detection approach. Thus, it is imperative

that the pore coordinates are detected correctly. The pore detection approaches can be broadly classified into feature-based approaches [2]–[13] and the learning-based approaches [15]–[18].

The early pore detection approaches [2]–[5] are based on skeletonization of fingerprint images. These approaches are evaluated on very high-resolution ( $\sim 2000$  dpi) fingerprint images and their performance is likely to be adversely affected by fingerprint degradation caused by skin conditions. As a solution to aforementioned challenges, Jain *et al.* [6] presented a hierarchical fingerprint recognition in which pores are detected by employing the Mexican-hat wavelet transform on the linear combination of original and enhanced fingerprint image. However, the presented pore detection approach in [6] is non-adaptive in nature. Later on, Zhao *et al.* [7] proposed an approach, in which the pores are extracted using the adaptive pore filtering method [19]. The authors have also demonstrated the usefulness of pores for biometric recognition using partial fingerprint images, which may not contain sufficient level-2 features [8], [9]. Teixeira and Leite [20] performed spatial distribution analysis of pores obtained by adaptive filtering using the directional field information and toggle mapping. The approaches presented in [7], [20] improved the pore detection accuracy but at the cost of increased computational complexity. Lemes *et al.* [12] proposed a pore detection approach with a low computational cost. Their approach is adaptive and handles variations in the pore size. Firstly, a binary fingerprint image is obtained through global thresholding. For every white pixel, the average valley width is then estimated by computing the distance to neighbouring dark pixels in each of the four directions. The average valley width is used to define the size of a mask centered on each white pixel. Bright pixels inside the mask are then used to define a local threshold  $T_{local}$  and a local radius  $r_{local}$ . Finally, a circle centered at each bright pixel with its local radius  $r_{local}$  is used to determine whether the bright pixel is part of a pore or not. Later on, Segundo and Lemes [13] improved the dynamic pore filtering approach [12] by considering the average ridge width in place of the average valley width to obtain the global and local radii, which are used in the same manner as in [12] to estimate the pore coordinates.

With the success of deep learning approaches in various computer vision tasks [21]–[23], researchers have focused on designing learning-based pore detection approaches. Labati *et al.* [15] proposed an approach for pore detection using a shallow CNN to generate a pore intensity map on which threshold is employed to obtain the pore coordinates. However,

V. Anand and V. Kanhangad are with the Discipline of Electrical Engineering, Indian Institute of Technology Indore, Indore 453552, India e-mail: phd1401202011@iiti.ac.in (V. Anand), kvivek@iiti.ac.in (V. Kanhangad).

the approach [15] does not provide any improvement in the pore detection over the existing feature-based techniques. Later on, Jang *et al.* [16] presented a pore detection approach by employing deep CNN consisting of 10 learnable layers. In their approach, pore label image is generated by considering the distance of the pixels from the pore coordinates. The deep CNN is trained to obtain the pore intensity map which is further processed to obtain the pore coordinates. DeepPore [16] provides a considerable improvement in the pore detection accuracy over the existing approaches. However, CNN network presented in [16] employed a plain CNN architecture with only 10 learnable layers and tested on a very small test set containing 6 fingerprint images only. Authors in [17] proposed a residual learning based CNN, referred to as DeepResPore, for detecting pores in high-resolution fingerprint images. Specifically, DeepResPore model consists of 18 layers containing 8 residual blocks. DeepResPore has been trained on a large labeled dataset containing 210,330 patches and evaluated on multiple test sets each containing 30 fingerprint images to ascertain its performance. Dahia and Segundo [18] employed fully convolutional neural network (FCN) for detecting pores in high-resolution fingerprint images. Authors in [18] have also provided a common protocol to evaluate the pore detection accuracy.

A review of the pore detection literature indicates that learning-based pore detection approaches achieve better performance than the feature-based pore detection approaches. However, all the existing learning-based pore detection approaches are trained and tested on the fingerprint images from the benchmark PolyU HRF datasets [24] only. Thus, the domain adaptability of existing learning-based pore detection approaches have not been examined in the past. To this end, we have generated an in-house pore ground truth dataset referred to as IITI-HRF-GT containing 20 fingerprint images of resolution 1000 dpi and the corresponding pore coordinates marked manually. The objectives of this work is to explore the domain adaptability of learning-based pore detection approaches on cross-sensor fingerprint images captured using a different fingerprint sensors. To the best of our knowledge, this is the first study of domain adaptability of learning-based pore detection approaches on the cross sensor fingerprint images.

The key contribution of this paper are as follows: this paper presents the first study of domain adaptability of the existing learning-based pore detection approaches on the cross-sensor fingerprint images. A cross-sensor pore ground truth (IITI-HRF-GT) is generated from fingerprint images of resolution 1000 dpi captured using the commercially available Biometrika HiScan-Pro fingerprint scanner. The in-house ground truth dataset used in this study will be made publicly available to further research in this area. Finally, as a solution for domain adaptability in pore detection, we have proposed an approach for detecting pores referred to as DeepDomainPore using unsupervised domain adaptation. Domain adaptability is achieved by incorporating the gradient reversal layer during the training phase.

The rest of this paper is organized as follows: Firstly, a brief introduction to the proposed methodology is presented in Section II followed by a detailed description of the domain

adversarial training of the proposed approach. Experimental results and discussion are presented in Section III. This section also presents detailed description of the dataset preparation for adversarial training the proposed model. Finally, Section IV presents our concluding remark.

## II. PROPOSED METHOD

In this paper, we present an automated pore detection approach referred to as DeepDomainPore capable of pore detection in cross-sensor fingerprint images. DeepDomainPore is combination of the residual learning-based CNN model DeepResPore [17] and the unsupervised domain adaptation approach [25] incorporated by embedding a gradient reversal layer during the training of DeepResPore model. The DeepDomainPore is trained using the labeled data from the source domain and an unlabeled data from the target domain. A schematic diagram of the proposed approach is presented in Fig. 1.

The domain adaptation is defined as the process of learning a discriminative classifier or predictor in the presence of a shift between the training and test distribution [25], [26]. In this paper, we present a learning-based pore detection approach which incorporates a domain adversarial learning during the training process. Let the PolyU HRF dataset [24] be treated as source domain  $S$ . For our experiments,  $S$  consists of fingerprint patches  $x_i^s$  and the pore label image  $y_i$  highlighting only the pore coordinates and its neighbourhood. On the other hand, the in-house high-resolution fingerprint dataset IITI-HRFP [27] containing fingerprint images of resolution 1000 dpi and size  $320 \times 240$  pixels be treated as target domain  $T$ . The target domain  $T$  contains unlabeled the fingerprint patches  $x_i^t$ . Sample fingerprint images from IITI-HRFP-GT and PolyU HRF pore ground truth (PolyU HRF GT) are presented in Fig. 2. As can be observed, there exist a significant difference in terms of resolution and pores between the fingerprint images of PolyU HRF and IITI-HRFP datasets. Thus, our objective is to design a learning-based pore detection approach which can handle the domain shift.

For training the DeepDomainPore, fingerprint patches are taken from both  $S$  and  $T$  domains. In order to have domain variability, each training sample  $x_i$  is assigned a domain label  $d_i$  as follows:

$$d_i = \begin{cases} 0, & \text{if } x_i \in S \\ 1, & \text{if } x_i \in T \end{cases} \quad (1)$$

As presented in Fig. 1, DeepDomainPore consists of DeepResPore [17] in the the feed forward network. In this work, we have included an additional batch normalization (BN) and rectified linear unit (ReLU) layer after the last convolutional layer of the DeepResPore model. The detailed architecture of the DeepResPore is presented in Table I. As can be observed, the output size of each layer is the same as that of the input. In order to achieve this, we have performed padding operation and have not employed pooling operation. A schematic diagram of the modified DeepResPore model is presented in Fig. 3. As depicted in Fig. 3, the modified DeepResPore model contains 4 residual blocks and additional

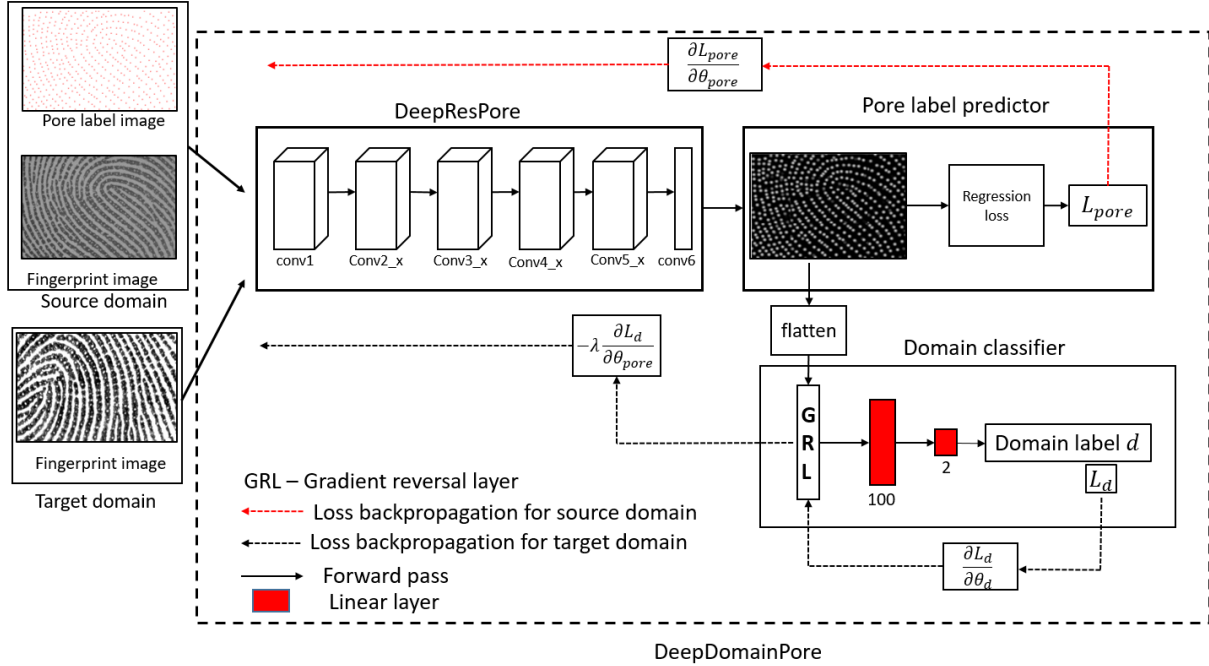


Fig. 1: Schematic diagram of the DeepDomainPore model

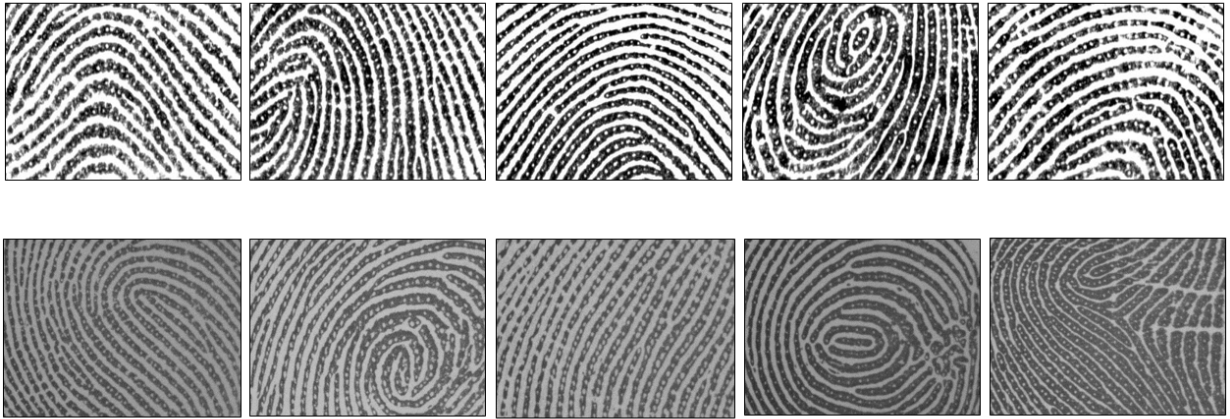


Fig. 2: Sample fingerprint images from IITI-GT (top) and PolyU HRF GT (bottom)

BN and ReLU layer are used with the last convolutional layer (conv6).

TABLE I: Architecture of DeepResPore

Layer name	output size	kernel
conv1	$80 \times 80$	$7 \times 7, 64, \text{stride } 1, \text{padding same}$
conv2_x	$80 \times 80$	$\begin{bmatrix} 3 \times 3, 64 \\ 3 \times 3, 64 \end{bmatrix} \times 2$
conv3_x	$80 \times 80$	$\begin{bmatrix} 3 \times 3, 128 \\ 3 \times 3, 128 \end{bmatrix} \times 2$
conv4_x	$80 \times 80$	$\begin{bmatrix} 3 \times 3, 256 \\ 3 \times 3, 256 \end{bmatrix} \times 2$
conv5_x	$80 \times 80$	$\begin{bmatrix} 3 \times 3, 512 \\ 3 \times 3, 512 \end{bmatrix} \times 2$
conv6	$80 \times 80$	$3 \times 3, 1$

DeepResPore generates a pore intensity map  $\hat{y}$  of the size same as that of the input fingerprint patch  $x_i$ . Let this mapping

and the parameters associated to it be represented as:

$$\hat{y} = f_P(X, \theta_{pore}) \quad (2)$$

The pore intensity map  $\hat{y}$  generated from the feed forward network  $f_P$ , is then compared with the pore label images  $y$  to obtain the loss  $L_{pore}$  as:

$$L_{pore} = \frac{1}{n} \sum_{i=1}^n (y_i - \hat{y}_i)^2 \quad (3)$$

For domain adaption, the pore intensity map  $\hat{y}$  generated from  $f_P$  is mapped to the domain label  $d$  by a domain classifier function  $f_D$  as follows:

$$\hat{d} = f_D(X_d, \theta_d) \quad (4)$$

During the learning phase, our goal is to minimize the pore-label loss  $L_{pore}$  on the annotated fingerprint images  $x_i^s$

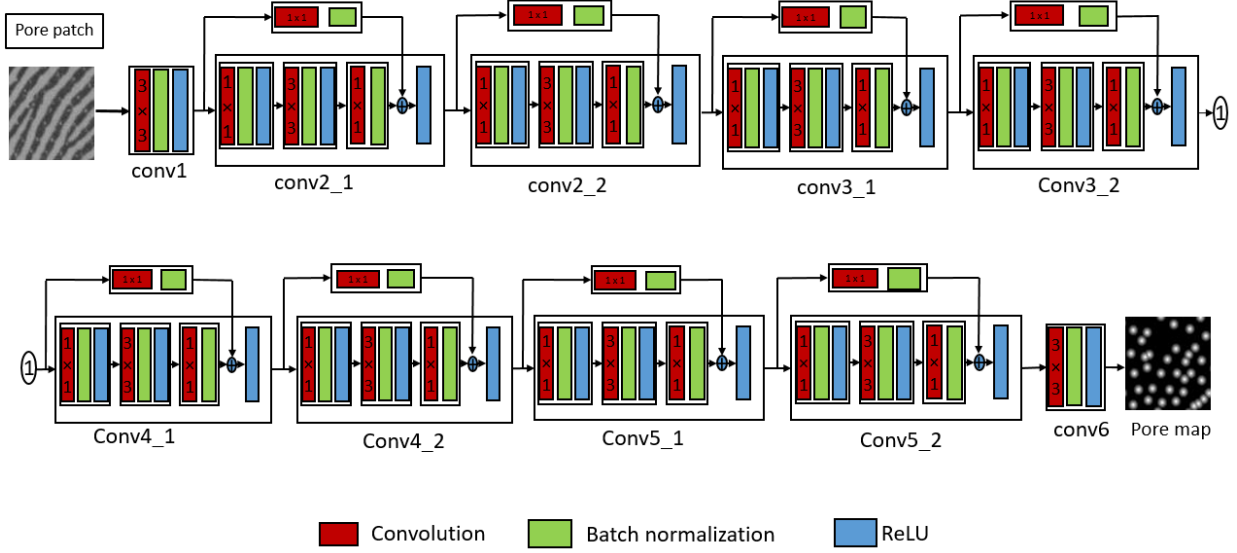


Fig. 3: Schematic diagram of DeepResPore showing generation of pore map from a given fingerprint patch

from the source domain which form a part of the training set  $X$ . The parameters  $\theta_{pore}$  of the feed forward network (DeepResPore) is optimized to minimize  $L_{pore}$  for fingerprint images from source domain. Simultaneously, our aim is to make the predictions  $\hat{y}$  from the DeepResPore model to be domain invariant. To this end, we have incorporated domain adversarial training [26] in the DeepResPore model and obtained the DeepDomainPore model. DeepDomainPore contain an additional domain classifier  $f_D$  which takes pore intensity map  $\hat{y}$  of size  $80 \times 80$  pixels generated from the  $f_P$  and employs a series of linear functions to obtain 1-dimensional vector, from which domain probability can be estimated by employing softmax function. Thus, during training, our objective is to obtain parameters  $\theta_{pore}$  of pore intensity map generation function  $f_P$  that minimizes the predicted pore loss  $L_{pore}$  and maximizes the domain classifier loss  $L_d$  to ensure domain invariability between the pore maps generated from the source and target domains. Further, we seek the parameters  $\theta_d$  of domain classifier that minimizes the loss of the domain classifier. The aforementioned objectives are summarized as the loss function as follows:

$$E(\theta_{pore}, \theta_d) = \frac{1}{n} \sum_{i=1}^n L_{pore}^i(\theta_{pore}) - \lambda \left[ \frac{1}{n} \sum_{i=1}^n L_d^i(\theta_{pore}, \theta_d) + \frac{1}{n'} \sum_{i=n+1}^N L_d^i(\theta_{pore}, \theta_d) \right] \quad (5)$$

In order to optimize eq. (5), we need to find the saddle point  $\hat{\theta}_{pore}$  and  $\hat{\theta}_d$  such that

$$\hat{\theta}_{pore} = \arg \min_{\theta_{pore}} E(\theta_{pore}, \hat{\theta}_d) \quad (6)$$

$$\hat{\theta}_d = \arg \max_{\theta_d} E(\hat{\theta}_{pore}, \theta_d) \quad (7)$$

A saddle point defined in (6)-(7) can be obtained as a stationary point of gradient updates of  $\theta_{pore}$  and  $\theta_d$  as follows:

$$\theta_{pore} \leftarrow \theta_{pore} - \mu \left( \frac{\partial L_{pore}^i}{\partial \theta_{pore}} - \lambda \frac{\partial L_d^i}{\partial \theta_{pore}} \right) \quad (8)$$

$$\theta_d \leftarrow \theta_d - \mu \frac{\partial L_d^i}{\partial \theta_d} \quad (9)$$

where  $\mu$  is the learning rate. The updates in equ. (8) can be achieved by introducing a special layer termed as **gradient reversal layer** [26]. The gradient reversal layer does not contain parameters associated with it. However, it has a meta-parameter  $\lambda$  (domain adaptation factor) associated with it. During forward pass the gradient reversal layer acts as an identity transform. On the other hand, during backpropagation, gradient reversal layer takes the gradient from the following layer and multiplies it with  $-\lambda$  and passes it to the preceding layer. Mathematically, the forward and the backpropagation of the gradient reversal layer can be represented by pseudo-functions as follows [26]:

$$R_\lambda(x) = x \quad (10)$$

$$\frac{dR_\lambda}{dx} = -\lambda I \quad (11)$$

In the proposed approach, the gradient reversal layer is employed between the DeepResPore model  $f_P$  and the domain classifier  $f_D$  as presented in Fig. 1. During the backpropagation pass through gradient reversal layer, partial derivative of domain classifier loss  $L_d$  with respect to the layer parameter  $\theta_{pore}$  i.e.  $\frac{\partial L_d}{\partial \theta_{pore}}$  is multiplied by  $-\lambda$  and then passed to DeepResPore model. During test phase, a test fingerprint image is first divided into non-overlapping patches of size  $80 \times 80$  pixels, which are then processed by DeepDomainPore model to generate the pore intensity map of same size as that of input patch which highlights only the pore coordinates and suppress the remaining details. These output pore intensity

maps are then combined to form the complete pore map of the same size as that of the input fingerprint image.

For a given test fingerprint image, DeepDomainPore generates a pore intensity map, in which pores appear clearly as grey-level blobs and rest of the fingerprint features are suppressed, as can be seen in Fig. 4. Also, it may be observed that the centers of the grey-level blobs (pores) correspond to the local maxima in the pore intensity map. Thus, we have employed a simple spatial filtering approach to estimate the pore coordinates [17]. In this approach, firstly, a maximum value map is obtained by filtering the pore intensity map with a maximum filter of window size  $5 \times 5$  pixels. Next, for every pixel in the pore intensity map, if its value is equal to the corresponding pixel value in the maximum value map and greater than a pre-defined threshold  $th_p$ , the corresponding pixel in the binary pore map is set to 1. If the aforementioned condition is not satisfied, the corresponding pixel in the binary pore map is set to zero. Sample fingerprint images from the target domain and their corresponding pore intensity map and binary pore map obtained by the proposed approach are presented in Fig. 4.

### III. EXPERIMENTAL RESULTS AND DISCUSSION

In this section, we first present the details of preparation of the dataset for examining the domain adversary on the learning-based pore detection approaches followed by the results of our experiments.

#### A. Dataset preparation

As presented in Section I, existing learning-based pore detection approaches have been trained and tested on the fingerprint images from PolyU HRF dataset [24]. Specifically, all the existing learning-based pore detection approaches have used the ground truth of pore coordinates provided in the PolyU HRF dataset which contains high-resolution fingerprint images of resolution 1200 dpi captured using a single sensor. Therefore, the performance of the learning-based pore detection approaches on an adversarial domain containing high-resolution fingerprint images from different sensor has not been evaluated in the past. The main reason behind this could be the unavailability of the ground truth of the pore coordinates of high-resolution fingerprint obtained from a different sensor. To this end, we have expanded the in-house IITI-HRF high-resolution fingerprint dataset [27] to include fingerprint images from 100 subjects. The current IITI-HRF high-resolution fingerprint dataset contains fingerprint images from 8 fingers (all fingers except the little fingers from both the hands), each contributing 8 impressions. These images are captured using the commercially available Biometrika HiScan-Pro fingerprint scanner. IITI-HRF dataset has two subsets, the first one contains the partial fingerprint images of size  $320 \times 240$  pixels, while the second one contains the full fingerprint images of size  $1000 \times 1000$  pixels. the details of IITI-HRF dataset is presented in Table II .

We have performed our experiment on IITI-HRFP dataset. Specifically, We have manually marked the pore coordinates

TABLE II: Details of the IITI-HRF dataset

Dataset	Resolution (dpi)	Image size (pixels)	Fingers	Total images
IITI-HRFP	1000	$320 \times 240$	800	6400
IITI-HRFC	1000	$1000 \times 1000$	800	6400

location for 20 fingers (randomly selected) to form the in-house ground truth, referred to as IITI-HRF-GT. Out of 20 fingerprint images from IITI-HRF-GT, 5 fingerprint images have been used for validation and fine tuning experiments and the remaining 15 fingerprint images are used for testing the DeepDomainPore model. On the other hand, all the impressions of remaining fingers ( $780 \times 8$ ) are used for training the DeepDomainPore as target domain  $T$ . We have divided the fingerprint images in  $T$  into non-overlapping patches of size  $80 \times 80$  pixels. Thus, we have a total of 74,880 fingerprint patches from  $T$  to train the DeepDomainPore model in domain adversarial manner. Furthermore, the training images for the source domain  $S$  are obtained from the fingerprint images from the PolyU HRF dataset for which the pore annotations are provided in [28]. Authors in [28] have provided pore annotation for 120 fingerprint images of size  $640 \times 480$  pixels from Polyu HRF dataset. Out of 120 fingerprint images, we have selected 90 fingerprint images from the first session as source training set. The images from source training set are divided into overlapping patches of size  $80 \times 80$  pixels with a step size of 10 pixels. Overall, we have a total of 210,330 fingerprint patches from  $S$  to train the DeepDomainPore model.

For training the DeepDomainPore model in a domain adversarial manner, we require training fingerprint images from source domain  $S$  with their corresponding pore label images  $I_P$  and training fingerprint images from target domain  $T$ . We have generated the pore label images from the annotated pores. Specifically, the pixels corresponding to the ground truth pore coordinates are marked as 1 in the pore label image and the pixels present inside the radius of 5 pixels from each of the ground truth pore are marked with the value equal to the distance from the center pore and the remaining pixels are marked as 0, in the following manner [16], [17]:

$$I_P(i, j) = \begin{cases} 1 - \frac{d_{pg}(i, j)}{5}, & \text{if } d_{pg}(i, j) < 5. \\ 0, & \text{otherwise.} \end{cases} \quad (12)$$

where  $I_P(i, j)$  is the label assigned to the pixel at  $(i, j)$  and  $d_{pg}(i, j)$  is the Euclidean distance between the pixel at  $(i, j)$  and the ground truth pore coordinates.

#### B. Experimental results

We have trained DeepDomainPore in an end-to-end manner to optimize the pore detection loss  $L_{pore}$  for the source domain fingerprint images and the domain classifier loss  $L_d$  for target domain fingerprint images. DeepDomainPore has been trained for 10 epochs (each containing 9360 iterations) using a batch size of 8 for both the source and target training sets and a learning rate of 0.0001. The number of epochs have been decided by considering the training loss and the average true detection rate on the validation set. The loss functions



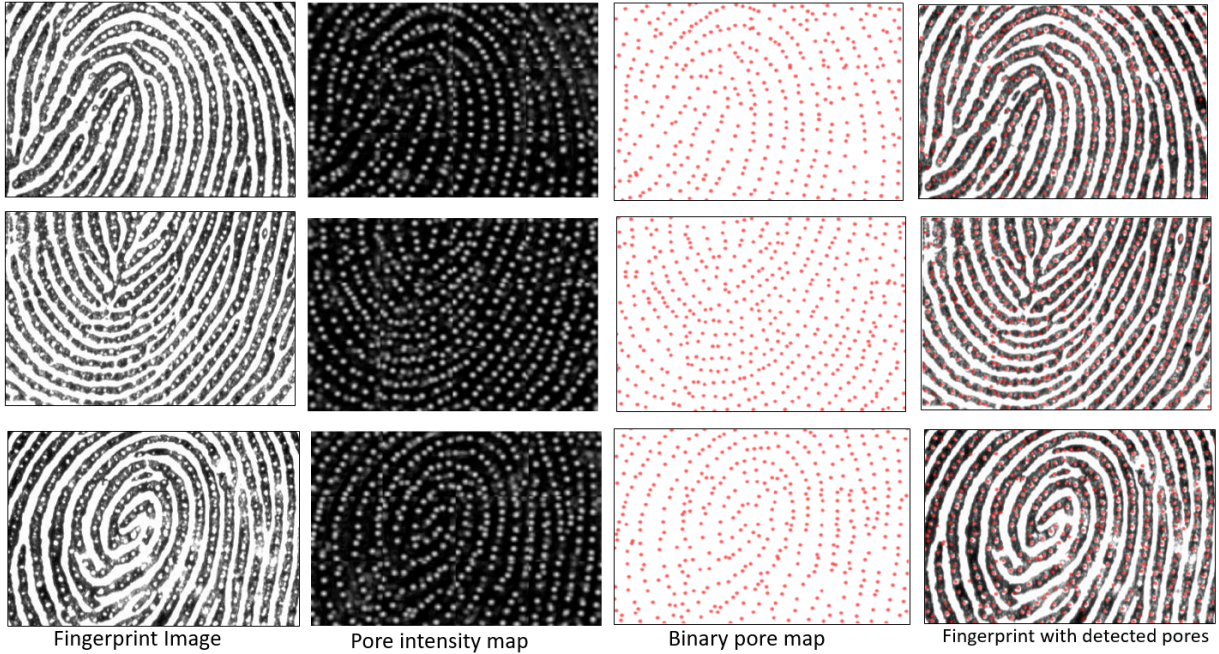


Fig. 4: Results from different stages of the proposed approach

have been optimized using the adaptive moment estimation (ADAM) [29]. The domain adaptation factor  $\lambda$  is set to 0.005. All our experiments have been performed using PyTorch [] in python environment on a computer with 3.60 GHz Intel core i7-6850K processor, 48 GB RAM and Nvidia GTX 1080 8 GB GPU.

The performance of all the approaches are evaluated using the following metrics: true detection rate  $R_T$  and false detection rate  $R_F$  [15]–[17].  $R_T$  is defined as the ratio of the true detected pores to the pores present in the ground truth.  $R_T$  can also be treated as the *recall* of the pore detection approach. On the other hand,  $R_F$  is defined as the ratio of the falsely detected pores to the total number of detected pores.  $R_F$  is equivalent to  $1 - \textit{precision}$  of the pore detection approach. We also report the F-score, which is harmonic mean of the *recall* and the *precision*. In addition, we present the receiver operating characteristic (ROC) curve to help ascertain the performance of the proposed approach in the cross sensor scenario.

In order to obtain the aforementioned performance metrics, it is quintessential how the detected pores are treated as true pores. To this end, we have employed the protocol presented in [18]. For a given fingerprint, let the detected pores and the corresponding ground truth pores be represented as  $P_d$  and  $P_g$ , respectively. Firstly, we compute the pair-wise Euclidean distance between  $P_d^i$  and  $P_g^j$  and store it in a distance matrix  $D_{pg}^{i,j}$ , for  $i = 1, 2, \dots, N$  and  $j = 1, 2, \dots, M$  where  $N$  and  $M$  are the number of detected pores and the ground truth pores, respectively. Next, we obtain the index of the minimum distance along each rows of the  $D_{pg}^{i,j}$ . These indices  $j' \in \{1, 2, \dots, M\}$  provide the coordinates of the nearest ground truth pore for each of the detected pores. Further, we determine the nearest detected pore to the obtained ground truth pore by examining the  $j'$ th column of the  $D_{pg}^{i,j}$  to find

the index  $i' \in \{1, 2, \dots, N\}$  of the minimum distance along the column. Finally, a detected pore  $P_d^i$  is considered as true pore only when  $i = i'$ , *i.e.* the detected pore has minimum distance with a ground truth pore and that ground truth pore must also has the minimum distance with that detected pore only.

To make a fair comparison, we have evaluated the existing approaches [16]–[18] and the proposed DeepDomainPore model on the test fingerprint images from IITI-HRF-GT. It should be noted that the existing approaches [16], [17] have been trained using the 210,330 fingerprint patches from the source domain. While, the approach in [18] has been trained on different segment of images obtained from the source domain only. We have also performed the pore detection in cross sensor domain through fine-tuning approach referred to as DeepResPore-FT. Specifically, we have fine-tuned the DeepResPore model by using the validation fingerprint images from the IITI-HRF-GT and retaining the weights of the trained DeepResPore model for all the layers except the last convolutional layer. The last convolutional layer is replaced with a new convolutional layer whose weights are learned using the cross sensor fingerprint images and the pore labels. The validation fingerprint images from IITI-HRF-GT are divided into overlapping patches of size  $80 \times 80$  pixels with a step size of 10 pixels. Thus, we have 2125 patches for fine-tuning experiment. The pore label image from the corresponding fingerprints are obtained by using the equ. 12. We have trained the DeepResPore-FT model for 20 epochs with a learning rate of 0.01.

The results from the cross sensor scenario experiments are presented in Table III. To make a fair comparison, we have fixed the  $R_F$  value  $\approx 19$  and computed the corresponding  $R_T$  and F-score for the proposed DeepDomainPore, DeepResPore-

TABLE III: Performance comparison with the existing methods in cross sensor scenario

Method	Metric		
	$R_T$	$R_F$	F-score
DeepPore [16]	86.34%	19.11%	83.23%
DeepResPore [17]	70.91%	19.13%	74.75%
Dahia and Segundo [18]	85.19%	29.09%	76.79%
DeepResPore-FT	85.89%	19.10%	82.70%
DeepDomainPore	<b>88.09%</b>	19.17%	<b>83.93%</b>

TABLE IV: Performance comparison with the existing methods on source sensor data

Method	Metric		
	$R_T$	$R_F$	F-score
DeepPore [16]	84.85%	2.52%	90.49%
DeepResPore [17]	85.00%	2.50%	90.44%
DeepDomainPore	<b>87.41%</b>	2.52%	<b>92.04%</b>

FT and the existing approaches [16], [17]. For the approach in [18], we have not been able to set the  $R_F$  value to 19. Therefore, we have reported the minimum  $R_F$  and the corresponding  $R_T$  and F-score of the approach [18]. As can be observed from the Table III, DeepDomainPore model which has been trained in a domain adversarial manner provide better results than all the existing approaches in a cross sensor scenario. To ascertain this superior performance, we have plotted ROC curves (please see Fig. 5) by varying the  $th_p$  values. These curves clearly indicate that the proposed approach achieves better  $R_T$  for low  $R_F$ , specifically, for  $R_F$  values below 25. The performance improvement in the cross sensor scenario is mainly be due to the domain adversarial training of the DeepDomainPore model.

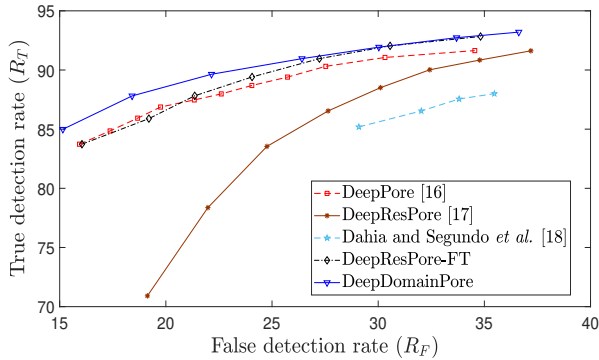


Fig. 5: A comparative analysis using ROC curves in cross sensor scenario

Further, we have also compared the performance of the DeepDomainPore with the existing approaches [16], [17] on fingerprint images from the source domain. For this set of experiments, the ground truth provided in PolyU HRF dataset [24] has been used as the test fingerprint images. Table IV presents the results obtained from this set of experiments. As performed in cross sensor scenario experiments, we have fixed the  $R_F$  value  $\approx 2.5$  and then reported the corresponding  $R_T$  and F-score. As can be seen the proposed approach performs better than the current state-of-the-art approaches on the test set from the source domain. To ascertain this superior performance, we have plotted ROC curves in Fig. 6 by varying the threshold  $th_p$ . These curves clearly indicate that

the proposed DeepDomainPore model trained with domain adversarial manner achieves better  $R_T$  for low  $R_F$  values.

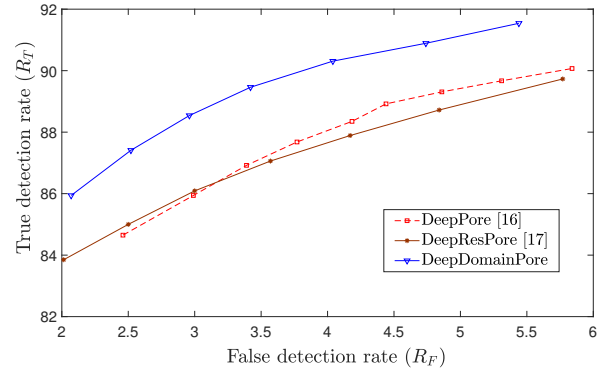


Fig. 6: A comparative analysis using ROC curves on source domain

Overall, the experimental results presented in this section indicate that the proposed DeepDomainPore model provides improvement in performance over the current state-of-the-art approaches for both the cross sensor scenario and the source domain scenario. Specifically, it achieves higher  $R_T$  for low  $R_F$  on both the datasets.

#### IV. CONCLUSION

In this paper, we have presented a learning based methodology for pore detection in cross-sensor high-resolution fingerprint images. Specifically, we have developed a CNN model named DeepDomainPore that generates a pore intensity map for the input fingerprint image. DeepDomainPore is a combination of residual learning-based CNN named DeepResPore and the unsupervised domain adaptation incorporated by embedding a gradient reversal layer between the DeepResPore and the domain classifier network and training the entire network in domain adversarial manner. The results of our evaluations on the cross sensor IITI-HRF-GT demonstrate the effectiveness of the proposed DeepDomainPore in detecting pores in high-resolution fingerprint images with a significant domain shift. Most importantly, the proposed DeepDomainPore model achieves state-of-the-art performances on both the source (PolyU HRF GT) and the target (IITI-HRF-GT) domain.

## REFERENCES

- [1] D. Zhang, F. Liu, Q. Zhao, G. Lu, and N. Luo, "Selecting a reference high resolution for fingerprint recognition using minutiae and pores," *IEEE Transactions on Instrumentation and Measurement*, vol. 60, no. 3, pp. 863–871, 2011.
- [2] J. D. Stosz and L. A. Aleya, "Automated system for fingerprint authentication using pores and ridge structure," in *Proc. SPIE*, vol. 2277, 1994, pp. 2277 – 2277 – 14.
- [3] A. R. Roddy and J. D. Stosz, "Fingerprint features-statistical analysis and system performance estimates," *Proc. of the IEEE*, vol. 85, no. 9, pp. 1390–1421, 1997.
- [4] K. Kryszczuk, A. Drygajlo, and P. Morier, "Extraction of level 2 and level 3 features for fragmentary fingerprint," *Second COST Action 275 Workshop*, pp. 83–88, 2004.
- [5] K. M. Kryszczuk, P. Morier, and A. Drygajlo, "Study of the distinctiveness of level 2 and level 3 features in fragmentary fingerprint comparison," in *Biometric Authentication*. Springer, 2004, pp. 124–133.
- [6] A. K. Jain, Y. Chen, and M. Demirkus, "Pores and ridges: high-resolution fingerprint matching using level 3 features," *IEEE Trans Pattern Anal. Mach. Intell.*, vol. 29, no. 1, pp. 15–27, Jan 2007.
- [7] Q. Zhao, L. Zhang, D. Zhang, and N. Luo, "Direct pore matching for fingerprint recognition," in *Advances in Biometrics*. Springer, 2009, pp. 597–606.
- [8] Q. Zhao, D. Zhang, L. Zhang, and N. Luo, "Adaptive fingerprint pore modeling and extraction," *Pattern Recognit.*, vol. 43, no. 8, pp. 2833 – 2844, 2010.
- [9] —, "High resolution partial fingerprint alignment using "porevalley" descriptors," *Pattern Recognition*, vol. 43, no. 3, pp. 1050 – 1061, 2010.
- [10] F. Liu, Q. Zhao, L. Zhang, and D. Zhang, "Fingerprint pore matching based on sparse representation," in *20th International Conference on Pattern Recognition*, Aug 2010, pp. 1630–1633.
- [11] F. Liu, Q. Zhao, and D. Zhang, "A novel hierarchical fingerprint matching approach," *Pattern Recognition*, vol. 44, no. 8, pp. 1604 – 1613, 2011.
- [12] R. d. P. Lemes, M. P. Segundo, O. R. P. Bellon, and L. Silva, "Dynamic pore filtering for keypoint detection applied to newborn authentication," *Proc. Int. Conf. on Pattern Recognition (ICPR)*, pp. 1698–1703, Aug 2014.
- [13] M. P. Segundo and R. d. P. Lemes, "Pore-based ridge reconstruction for fingerprint recognition," in *Proc. IEEE Conf. on Computer Vision and Pattern Recognition Workshops (CVPRW)*, 2015, pp. 128–133.
- [14] V. Anand and V. Kanhangad, "Pore based indexing for high-resolution fingerprints," in *IEEE International Conference on Identity, Security and Behavior Analysis (ISBA)*, Feb 2017, pp. 1–6.
- [15] R. D. Labati, A. Genovese, E. Muñoz, V. Piuri, and F. Scotti, "A novel pore extraction method for heterogeneous fingerprint images using convolutional neural networks," *Pattern Recognit. Lett.*, 2017.
- [16] H. U. Jang, D. Kim, S. M. Mun, S. Choi, and H. K. Lee, "DeepPore: Fingerprint pore extraction using deep convolutional neural networks," *IEEE Signal Process. Lett.*, vol. 24, no. 12, pp. 1808–1812, Dec 2017.
- [17] V. Anand and V. Kanhangad, "Pore detection in high-resolution fingerprint images using deep residual network," *Journal of Electronic Imaging*, vol. 28, no. 2, pp. 1 – 4 – 4, 2019.
- [18] G. Dahia and M. P. Segundo, "Improving fingerprint pore detection with a small FCN," *CoRR*, vol. abs/1811.06846, 2018. [Online]. Available: <http://arxiv.org/abs/1811.06846>
- [19] Q. Zhao, L. Zhang, D. Zhang, N. Luo, and J. Bao, "Adaptive pore model for fingerprint pore extraction," in *2008 19th International Conference on Pattern Recognition*, Dec 2008, pp. 1–4.
- [20] R. F. S. Teixeira and N. J. Leite, "Improving pore extraction in high resolution fingerprint images using spatial analysis," *Proc. IEEE Int. Conf. on Image Processing (ICIP)*, pp. 4962–4966, 2014.
- [21] F. Schroff, D. Kalenichenko, and J. Philbin, "Facenet: A unified embedding for face recognition and clustering," in *IEEE Conference on Computer Vision and Pattern Recognition (CVPR)*, June 2015, pp. 815–823.
- [22] O. M. Parkhi, A. Vedaldi, and A. Zisserman, "Deep face recognition," in *Proceedings of the British Machine Vision Conference (BMVC)*. BMVA Press, September 2015, pp. 41.1–41.12.
- [23] E. Simo-Serra, E. Trulls, L. Ferraz, I. Kokkinos, P. Fua, and F. Moreno-Noguer, "Discriminative learning of deep convolutional feature point descriptors," in *IEEE International Conference on Computer Vision (ICCV)*, Dec 2015, pp. 118–126.
- [24] "PolyU HRF Database," Hong kong, 2009, [http://www4.comp.polyu.edu.hk/~biometrics/HRF/HRF\\_old.htm](http://www4.comp.polyu.edu.hk/~biometrics/HRF/HRF_old.htm).
- [25] Y. Ganin and V. Lempitsky, "Unsupervised domain adaptation by backpropagation," in *Proceedings of the 32nd International Conference on Machine Learning*, Jul 2015, pp. 1180–1189.
- [26] Y. Ganin, E. Ustinova, H. Ajakan, P. Germain, H. Larochelle, F. Laviolette, M. Marchand, and V. Lempitsky, "Domain-adversarial training of neural networks," *J. Mach. Learn. Res.*, vol. 17, no. 1, pp. 2096–2030, Jan 2016.
- [27] V. Anand and V. Kanhangad, "Pore-based indexing for fingerprints acquired using high-resolution sensors," *Pattern Analysis and Applications*, Mar 2019.
- [28] R. F. S. Teixeira and N. J. Leite, "A new framework for quality assessment of high-resolution fingerprint images," *IEEE Trans on Pattern Anal Mach Intell*, vol. 39, no. 10, pp. 1905–1917, Oct 2017.
- [29] D. P. Kingma and J. Ba, "Adam: A method for stochastic optimization." *CoRR*, vol. abs/1412.6980, 2014.